Determination of Waveguide Group Index Using Integrated Mach-Zehnder Interferometer

Bin Lu (edX username: BL_2507_V8GT)

December 2, 2025

Abstract

Silicon photonics enables dense integration of optical circuits with CMOS technology, supporting high-speed and low-cost communication. A critical design parameter is the waveguide group index, which governs dispersion and device bandwidth. In this work, we present theoretical modeling, simulation, fabrication, and characterization of silicon strip waveguides and Mach–Zehnder interferometers (MZIs). Using MODE and INTERCONNECT simulations, we extract effective and group indices, develop compact models, and study free spectral range (FSR) as a function of interferometer imbalance. Fabricated devices are experimentally tested, and measured spectra are used to extract the group index, allowing direct comparison with simulation results.

1 Introduction

In recent decades, silicon photonics has emerged as a leading technology for high-speed data transfer and on-chip signal processing. Using advanced CMOS fabrication processes, silicon photonics allows low-cost, high-density integration of optical components with electronic circuits. Many of the fundamental functionalities of silicon photonic devices, such as optical modulation, switching, and filtering,[1,2] rely on precise control of the waveguide group refractive index, which governs wave propagation and strongly influences device bandwidth. Accurate determination of the group index is therefore essential for the design and optimization of silicon photonic circuits. In this report, we present both simulation models and theoretical analysis of integrated silicon photonic circuits, with the ultimate goal of experimentally determining the group index of silicon waveguides. Our primary test structure is the Mach–Zehnder interferometer (MZI), a versatile and widely used interferometric device that allows precise measurement of the free spectral range (FSR) and, from it, the group index. MZIs also serve as fundamental building blocks for more advanced photonic circuits, including wavelength-selective switches, and finite impulse response filters. [3-5]

2 Theory

2.1 Waveguide Compact Model

The propagation of light in a silicon waveguide is characterized by the effective refractive index $n_{\text{eff}}(\lambda)$, which varies with wavelength due to material and waveguide dispersion. $n_{\text{eff}}(\lambda)$ can be described by a compact model of low-order polynomials around the design wavelength λ_0:

$$n_{\text{eff}}(\lambda) \approx a_0 + a_1(\lambda - \lambda_0) + a_2(\lambda - \lambda_0)^2 \tag{1}$$

Accordingly, the group index can be defined as

$$n_g(\lambda) = n_{\text{eff}}(\lambda) - \lambda \frac{dn_{\text{eff}}}{d\lambda}. \tag{2}$$

This expression captures the dispersion of the waveguide and is essential for circuit-level modeling.

2.2 Mach–Zehnder Interferometer Transfer Function

The Mach–Zehnder interferometer (MZI) consists of an input splitter, two branches of different path lengths, and an output combiner. For an input field E_i and equal splitting of light, the electric fields in the two branches are given by

$$E_1 = \frac{E_i}{\sqrt{2}} e^{-j\beta L_1}, \qquad E_2 = \frac{E_i}{\sqrt{2}} e^{-j\beta L_2}, \tag{3}$$

where $\beta = \frac{2\pi}{\lambda} n_{\text{eff}}(\lambda)$ is the propagation constant, and L_1, L_2 are the respective arm lengths.

At the output combiner, the superposed field is

$$E_o = \frac{1}{2} E_i \left(e^{-j\beta L_1} + e^{-j\beta L_2} \right). \tag{4}$$

The normalized transmission intensity of the MZI is therefore

$$T(\lambda) = \frac{I_o}{I_i} = \frac{1}{2} \left[1 + \cos(\beta \Delta L) \right], \tag{5}$$

where $\Delta L = L_2 - L_1$ is the imbalanced arm length of the MZI.

2.3 Free Spectral Range and Group Index Extraction

Given the imbalanced interferometer transfer function, the periodicity of the spectral response, known as the free spectral range (FSR), is expressed as

$$FSR(\lambda) = \frac{\lambda^2}{n_g(\lambda)\, \Delta L}. \tag{6}$$

From this relation, the waveguide group index can be experimentally determined as

$$n_g(\lambda) = \frac{\lambda^2}{FSR(\lambda)\,\Delta L}. \tag{7}$$

Thus, by constructing MZIs with known imbalances (ΔL) and measuring their transmission spectra, the group index can be accurately determined and compared with simulation results.

3 Modelling and Simulation

The silicon strip waveguide was simulated using Lumerical MODE. The geometry consists of a fixed height of $h_0 = 220$ nm and widths of $w_0 = 500$ nm.

The simulated mode profiles of the waveguide are shown in Fig. 1. The fundamental TE mode exhibits strong confinement within the silicon core. In our analysis, we focus on the fundamental quasi-TE polarization mode.

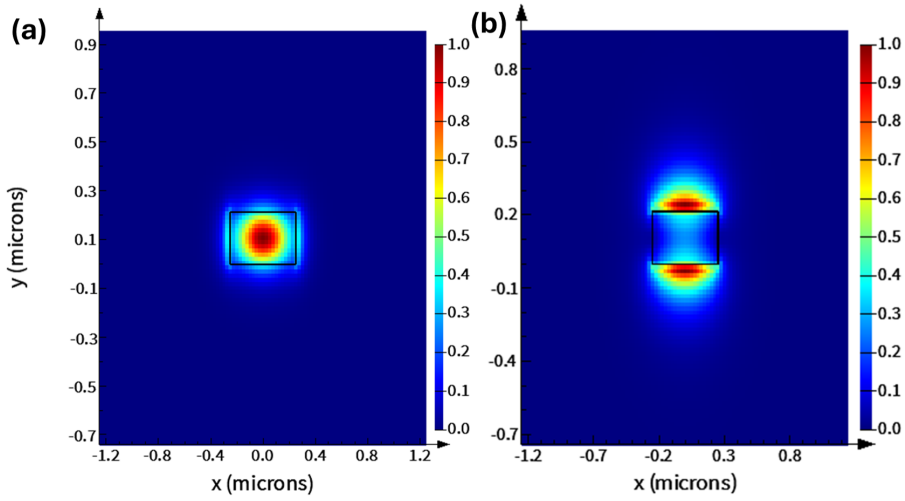

Figure 1: Simulated slab waveguide mode profiles: (a) TE mode, (b) TM mode at λ 1550 nm.

A wavelength sweep from 1500 nm to 1600 nm was performed to extract the effective index $n_{\text{eff}}(\lambda)$ and the group index $n_g(\lambda)$. The results are plotted in Fig. 2. A compact model was obtained by fitting the effective index to equation (1) at $\lambda_0 = 1550$ nm:

$$n_{\text{eff}}(\lambda) = 2.45 - 1.13(\lambda - \lambda_0) - 0.04(\lambda - \lambda_0)^2. \tag{8}$$

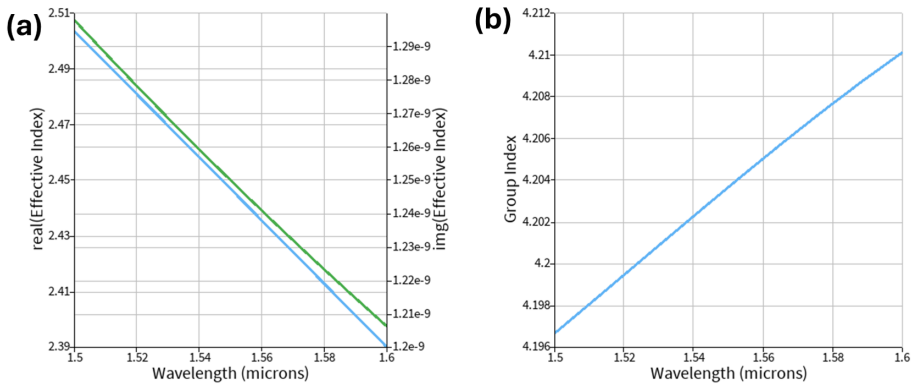

Figure 2: (a) Effective index $n_{\text{eff}}(\lambda)$ and (b) group index $n_g(\lambda)$ versus wavelength.

3.1 Modeling of Mach–Zehnder Interferometer

The Mach–Zehnder Interferometer (MZI) was modeled in Lumerical INTERCONNECT. It consists of two Y-branch splitters connected by waveguides of different lengths L_1 and L_2, as shown schematically in Fig. 3.

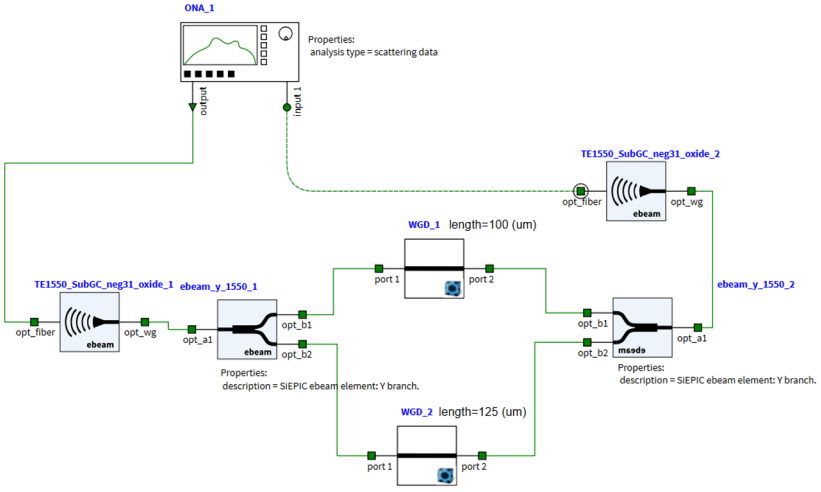

Figure 3: Schematic of the Mach–Zehnder interferometer circuit.

3.2 Parameter Variation Study

Several MZIs were simulated with different path length imbalances ΔL to investigate the dependence of the free spectral range (FSR) on ΔL. The expected

and simulated FSR values are summarized in Table 1. In the design file, we also included additional structures for testing, e.g., beam splitters based on broadband directional coupler (BDC) as well as Michelson interferometer.

Table 1: FSR v.s. ΔL.

ΔL (μm)	Simulated FSR (nm)
25	22.5
50	11.4
75	7.7
100	5.7
125	4.6

3.3 Transmission Spectra

Figure 4 shows the simulated spectra for several values of ΔL. As expected, increasing ΔL results in a smaller FSR, in good agreement with theory. The relationship between FSR and ΔL is summarized in Fig. 5.

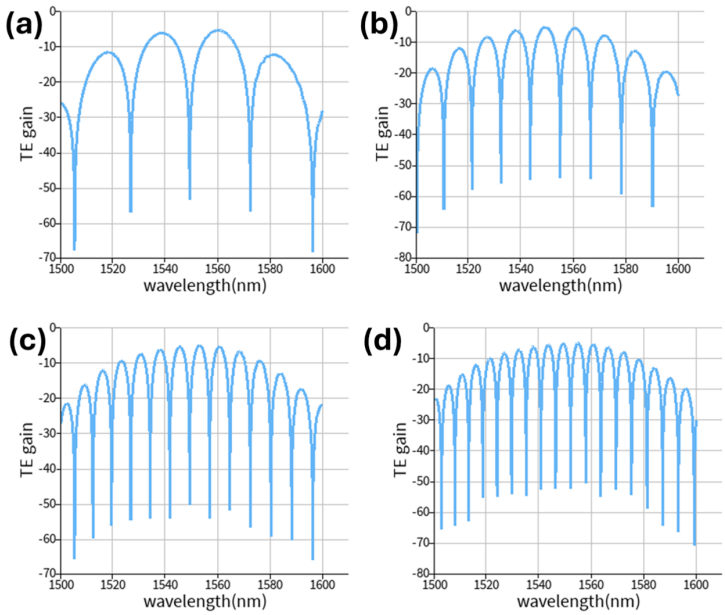

Figure 4: Simulated spectrum of the MZIs of different ΔL: (a) 25 μm, (b) 50 μm, (c) 75 μm, (d) 100 μm.

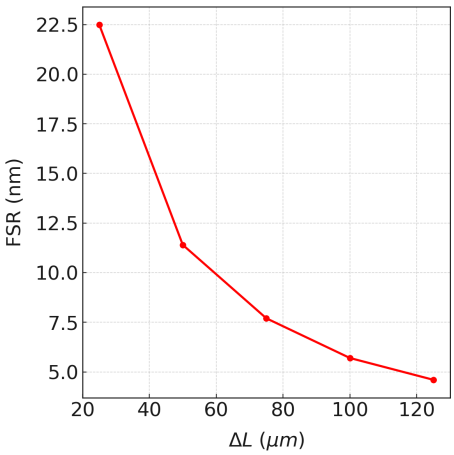

Figure 5: FSR versus ΔL.

4 Manufacturing Variability

The nominal dimensions of our waveguide design are fixed at $h_0 = 220$ nm and $w_0 = 500$ nm. In reality, structural variations will occur during fabrication processes, including thickness non-uniformity in the silicon device layer and variations in width introduced during resist development and the etching process. Such structural variations can cause significant changes in device performance. For robust design and measurement data analysis, the consequences of variations in the structural parameters should be taken into account. Here, we find extremes of structural parameters of $h_{\min} = 215.3$ nm, $h_{\max} = = 223.1$ nm, $w_{\min} = = 470$ nm, and $w_{\max} = = 510$ nm, as illustrated in Fig. 6. We perform a corner analysis in Lumerical MODE to determine the effective and group index of our waveguide design. The TE mode effective index n_{eff} and group index n_{g} as a function of the wavelength λ are plotted in Fig. 7. We fit n_{eff} of different cross sections in the corner analysis to the waveguide compact model, Eq. 1. The calculated transmission spectra of an MZI of $\Delta L = 25\mu$m are shown in Fig. 8. The corresponding values are listed in Table 2.

Table 2: Corner Analysis

(width, height) [nm]	$n_{\text{g}}(1.55\ \mu\text{m})$	FSR [nm])
(500, 220)	4.203	22.86
(510, 223)	4.187	22.90
(510, 215)	4.149	22.93
(470, 215)	4.252	22.46
(470, 223)	4.260	22.45

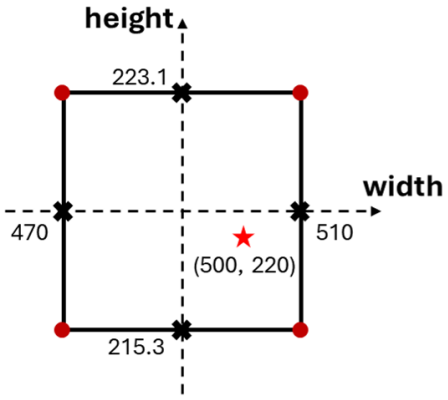

Figure 6: Illustration of the corner analysis for manufacturing variability.

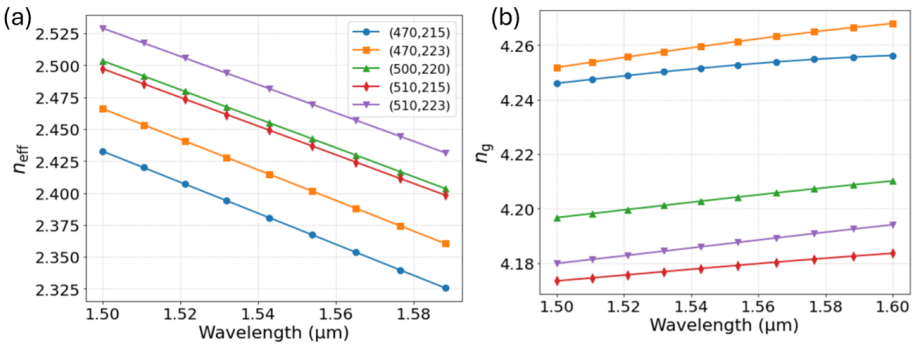

Figure 7: Waveguide refractive indices, (a) n_{eff} and (b) n_{g}, from the corner analysis.

5 Fabrication

The devices were fabricated using 100 keV Electron Beam Lithography [2]. The fabrication used silicon-on-insulator wafer with 220 nm thick silicon on 3 μm thick silicon dioxide. The substrates were 25 mm squares diced from 150 mm wafers. After a solvent rinse and hot-plate dehydration bake, hydrogen silsesquioxane resist (HSQ, Dow-Corning XP-1541-006) was spin-coated at 4000 rpm, then hotplate baked at 80 °C for 4 minutes. Electron beam lithography was performed using a JEOL JBX-6300FS system operated at 100 keV energy, 8 nA beam current, and 500 μm exposure field size. The machine grid used for shape placement was 1 nm, while the beam stepping grid, the spacing between dwell points during the shape writing, was 6 nm. An exposure dose of 2800 μC/cm2 was used. The resist was developed by immersion in 25% tetramethylammonium hydroxide for 4 minutes, followed by a flowing deionized water rinse for 60

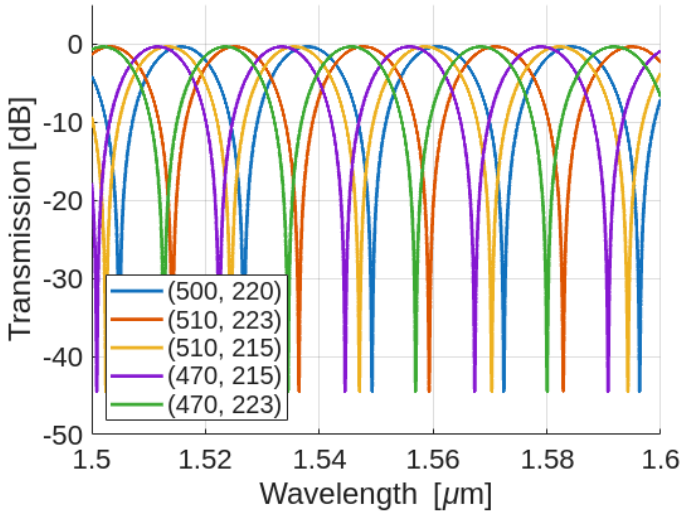

Figure 8: Waveguide refractive indices, (a) n_{eff} and (b) n_{g}, from the corner analysis.

s, an isopropanol rinse for 10 s, and then blown dry with nitrogen. The silicon was removed from unexposed areas using inductively coupled plasma etching in an Oxford Plasmalab System 100, with a chlorine gas flow of 20 sccm, pressure of 12 mT, ICP power of 800 W, bias power of 40 W, and a platen temperature of 20 °C, resulting in a bias voltage of 185 V. During etching, chips were mounted on a 100 mm silicon carrier wafer using perfluoropolyether vacuum oil.

6 Experimental Data

To characterize the devices, a custom-built automated test setup [3] with automated control software written in Python was used (`http://siepic.ubc.ca/probestation`). An Agilent 81600B tunable laser was used as the input source and Agilent 81635A optical power sensors as the output detectors. The wavelength was swept from 1500 to 1600 nm in 10 pm steps. A polarization maintaining (PM) fibre was used to maintain the polarization state of the light, to couple the TE polarization into the grating couplers [4]. A 90^{o} rotation was used to inject light into the TM grating couplers [4]. A polarization maintaining fibre array was used to couple light in/out of the chip [www.plcconnections.com].

Due to the limited bandwidth of the grating couplers, the transmission spectra are curved. We perform a baseline correction by polynomial fitting to the curved transmission spectra of a loop-back structure, Fig. 9 (a) and (b). After

the baseline correction, we obtain flattened transmission spectra, Fig. 9 (c) and (d).

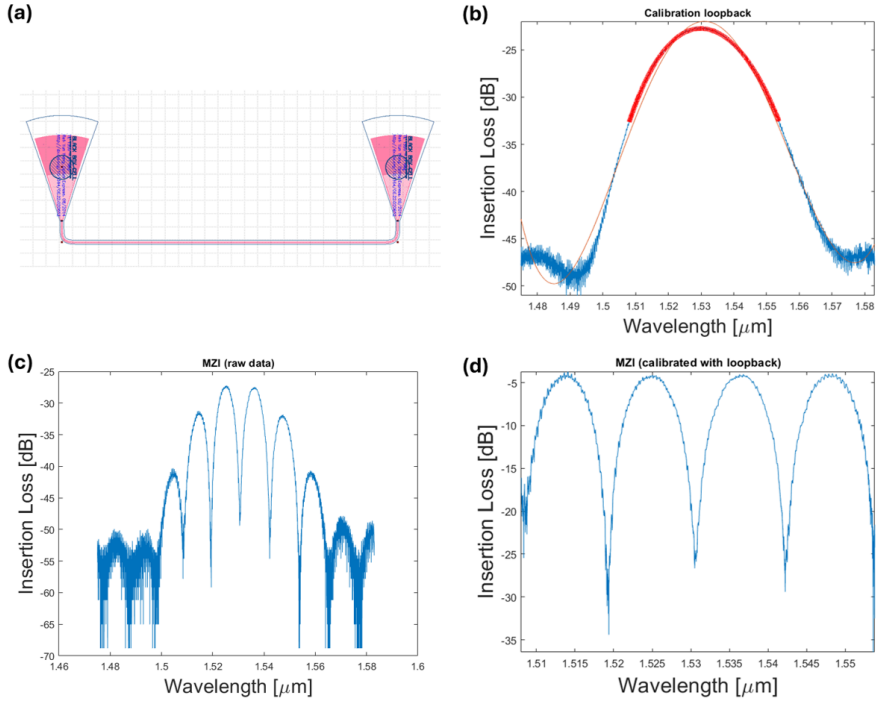

Abbildung 9: (a) Design layout of a loop-back structure. (b) The transmission spectrum of the loop-back structure with polynomial fitting. (c) The untreated and (d) calibrated transmission spectrum of an MZI of ΔL 50 μm.

7 Analysis

The calibrated spectra are then fitted to

$$T(\lambda) = 10\log_{10}\left(\frac{1}{4}\left|1+\exp\left(-i\beta(\lambda)\Delta L-\frac{\alpha\Delta L}{2}\right)\right|^2\right)+b, \tag{9}$$

where α is the waveguide loss, b is the insertion loss, and $\beta(\lambda)$ is propagation constant. Fig. 10 (a) shows the calibrated transmission spectrum with fitting of an MZI of ΔL 50 μm. The wavelength dependent group index obtained by fitting the transmission spectrum is plotted in Fig. 10 (b). Table 3 summarizes the group indices and FSR values from fitting the experimental data of MZIs with different ΔL. All n_g values fall into the range obtained in corner analysis (form 4.149 to 4.260). The average n_g of all five devices is 4.208. All FSR values fall within 3% deviation from the simulation results, Table 1.

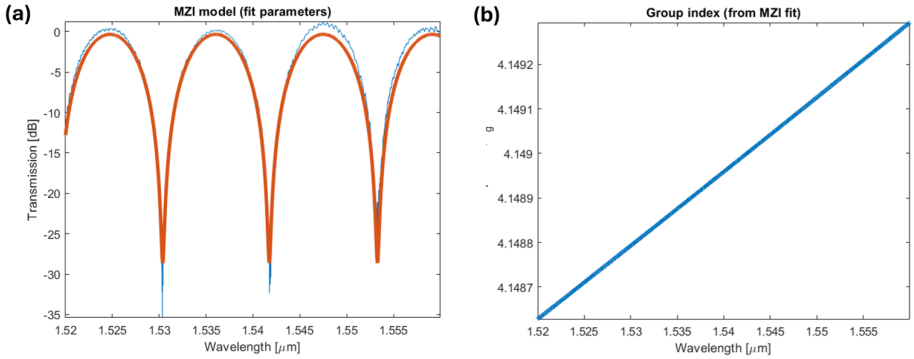

Abbildung 10: (a) Fitted transmission spectrum of an MZI ΔL 50 μm. (b) The group index obtained from the pectrum fitting.

Tabelle 3: Summary of experimental results for the MZIs

ΔL [μm]	$n_{\mathrm{g}}(1.55\ \mu\mathrm{m})$	FSR [nm])
25	4.252	22.4
50	4.151	11.6
75	4.184	7.5
100	4.186	5.7
125	4.242	4.5

8 Conclusion

In this report, we determined the group index of silicon strip waveguides using MZIs. Fabricated devices were characterized using a broadband transmission measurement setup, and baseline-corrected spectra enabled accurate extraction of the free spectral range. The resulting group indices ranged from 4.15 to 4.26 across all MZI geometries, with an average value of $n_g = 4.208$, consistent with simulation and manufacturing corner analysis. The measured free spectral ranges agreed with theory within 3% error. These results confirm that the fabricated silicon waveguides closely match the intended design and demonstrate that MZI-based interferometric metrology is a reliable technique for characterizing dispersion in silicon photonic waveguides.

9 Acknowledgements

We acknowledge the edX UBCx Phot1x Silicon Photonics Design, Fabrication and Data Analysis course, which is supported by the Natural Sciences and Engineering Research Council of Canada (NSERC) Silicon Electronic-Photonic Integrated Circuits (SiEPIC) Program. The devices were fabricated by Richard Bojko at the University of Washington Washington Nanofabrication Facility,

part of the National Science Foundation's National Nanotechnology Infrastructure Network (NNIN), and Cameron Horvath at Applied Nanotools, Inc. Enxiao Luan performed the measurements at The University of British Columbia. We acknowledge Lumerical Solutions, Inc., Mathworks, Mentor Graphics, Python, and KLayout for the design software.

References

1. Chrostowski L, Hochberg M (2015) Silicon Photonics Design. Cambridge University Press (CUP)

2. Bojko RJ, Li J, He L, et al. (2011) Electron beam lithography writing strategies for low loss high confinement silicon optical waveguides. Journal of Vacuum Science & Technology B: Microelectronics and Nanometer Structures 29:06F309. https://doi.org/10.1116/1.3653266

3. Chrostowski L, Hochberg M Testing and packaging. In: Silicon Photonics Design. Cambridge University Press (CUP), pp 381–405

4. Wang Y, Wang X, Flueckiger J, et al. (2014) Focusing sub-wavelength grating couplers with low back reflections for rapid prototyping of silicon photonic circuits. Opt Express 22:20652. https://doi.org/10.1364/oe.22.020652